Critical role of Aquaporin-1 and telocytes in infantile hemangioma response to propranolol beta blockade

François Moisan[a,1], Sandra Oucherif[a], Priscilla Kaulanjan-Checkmodine[a], Sorilla Prey[a,b], Benoît Rousseau[c], Marc Bonneu[d], Stéphane Claverol[d], Etienne Gontier[e], Sabrina Lacomme[e], Lea Dousset[a,b], Thierry Couffinhal[f], Jerome Toutain[g], Maya Loot[h], Muriel Cario-André[a,i], Marie-Laure Jullié[j], Christine Léauté-Labrèze[a,b,i], Alain Taieb[a,b,i], and Hamid Reza Rezvani[a,i]

[a]Inserm, Biothérapie des Maladies Génétiques Inflammatoires et Cancers (BMGIC), UMR 1035, University of Bordeaux, F-33076 Bordeaux, France; [b]Service de Dermatologie Adulte et Pédiatrique, Centre Hospitalier Universitaire (CHU) de Bordeaux, F-33000 Bordeaux, France; [c]Animalerie A2, University of Bordeaux, F-33000 Bordeaux, France; [d]Plateforme de protéomique, Centre de Génomique Fonctionnelle de Bordeaux, University of Bordeaux, F-33076 Bordeaux, France; [e]Bordeaux Imaging Center (BIC)–Electron Microscopy Unit, University of Bordeaux, F-33076 Bordeaux, France; [f]Inserm U 1034, University of Bordeaux, F-33600 Pessac, France; [g]Service de Génétique Médicale, CHU de Bordeaux, F-33000 Bordeaux, France; [h]Service de Chirurgie Pédiatrique, CHU de Bordeaux, F-33000 Bordeaux, France; [i]Centre de Référence pour les Maladies Rares de la Peau, CHU Bordeaux, F-33000 Bordeaux, France; and [j]Service d'anatomopathologie, CHU de Bordeaux, F-33000 Bordeaux, France

Edited by Napoleone Ferrara, University of California San Diego, La Jolla, CA, and approved December 15, 2020 (received for review September 14, 2020).

Propranolol, a nonselective β-adrenergic receptor (ADRB) antagonist, is the first-line therapy for severe infantile hemangiomas (IH). Since the incidental discovery of propranolol efficacy in IH, preclinical and clinical investigations have shown evidence of adjuvant propranolol response in some malignant tumors. However, the mechanism for propranolol antitumor effect is still largely unknown, owing to the absence of a tumor model responsive to propranolol at nontoxic concentrations. Immunodeficient mice engrafted with different human tumor cell lines were treated with anti-VEGF bevacizumab to create a model sensitive to propranolol. Proteomics analysis was used to reveal propranolol-mediated protein alteration correlating with tumor growth inhibition, and Aquaporin-1 (AQP1), a water channel modulated in tumor cell migration and invasion, was identified. IH tissues and cells were then functionally investigated. Our functional protein association networks analysis and knockdown of ADRB2 and AQP1 indicated that propranolol treatment and AQP1 down-regulation trigger the same pathway, suggesting that AQP1 is a major driver of beta-blocker antitumor response. Examining AQP1 in human hemangioma samples, we found it exclusively in a perivascular layer, so far unrecognized in IH, made of telocytes (TCs). Functional in vitro studies showed that AQP1-positive TCs play a critical role in IH response to propranolol and that modulation of AQP1 in IH-TC by propranolol or shAQP1 decreases capillary-like tube formation in a Matrigel-based angiogenesis assay. We conclude that IH sensitivity to propranolol may rely, at least in part, on a cross talk between lesional vascular cells and stromal TCs.

hemangioma | propranolol | telocyte | aquaporin-1 | angiogenesis

Infantile hemangioma (IH), the most frequent tumor of infancy affecting 1 to 5 out of 100 newborns, is a noncongenital benign vascular tumor. Although most IHs are small, inconsequential, and regress spontaneously in many cases, medical treatment is needed in at least 15% of cases. The current first-line therapy for severe IH is systemic propranolol, a nonselective β-adrenergic receptor (ADRB) antagonist (1). Three subtypes of ADRBs (ADRB1, ADRB2, and ADRB3), which are coded by three distinct genes, belong to the superfamily of G protein–coupled receptors. They are characterized by a pocket containing binding sites for agonists (e.g., adrenaline and noradrenaline) and competitive antagonists (e.g., propranolol and timolol) (2). Although a role for ADRB in cancer progression was suggested long ago (3), our serendipitous observation of the efficacy of propranolol in treating IH (4) prompted many researchers to explore the anticancer properties of β-blockers.

Although the therapeutic effect of propranolol is thought to be due to its ability to affect vasoconstriction, endothelial cell (EC) apoptosis, and/or inhibition of angiogenesis by modulating vascular endothelial growth factors (5, 6), the precise mechanism of its action is still under debate and largely unknown. Propranolol has been shown to have a growth inhibitory effect as a monotherapy on hemangioma cells in vitro (7–9). Nevertheless, growth inhibition was observed at doses 100- to 1,000-times higher than the plasmatic dose measured in treated IH patients (i.e., never above 0.5 μM) (10). It is then difficult to make the assumption that the effect of propranolol in IH can be mimicked and studied with such unrealistic doses. Indeed, the absence of an in vivo IH model that has shown a tumor growth inhibition induced by propranolol as well as difficulties in accessing IH patient samples before and after treatment have jointly hindered the quest to reveal its mechanism of action. Although several attempts have been made to create an in vivo IH model, a convincing antitumor effect of propranolol is still lacking (11–15). Of note, Lee et al. showed an effect of propranolol on vascular volume in a model of hemangioma cell–formed vessels in mice but without studying the effect on tumor growth (15). Considering this global effort and given the potential interest to identify a biomarker of malignant tumors sensitive to propranolol, we decided to explore the antitumor effect of propranolol in

Significance

Although a role for β-adrenergic receptor (ADRB) in cancer progression was suggested a long time ago, our serendipitous observation of the propranolol efficacy in treating infantile hemangioma (IH) has driven attention in exploring the antitumor properties of β-blockers. We identified Aquaporine-1 (AQP1) as a player in antitumor propranolol response and as a histological marker of IH vascular structures including telocytes, which are dendritic cells that form a distinctive peripheral layer in IH. We conclude that IH sensitivity to propranolol may rely, at least in part, on a cross talk between lesional vascular cells and stromal telocytes.

Author contributions: F.M., A.T., and H.R.R. designed research; F.M. and S.O. performed research; P.K.-C., S.P., B.R., M.B., S.C., E.G., S.L., L.D., T.C., J.T., M.L., M.C.-A., M.-L.J., and C.L.-L. contributed new reagents/analytic tools; and F.M., S.O., A.T., and H.R.R. analyzed data and wrote the paper.

Competing interest statement: A patent has been granted for the use of beta-blockers in infantile capillary hemangiomas, with A.T. and C.L.-L. as inventors and Bordeaux University and Bordeaux University Hospital as owners of the patent. None of the authors have any other financial interests related to this work.

This article is a PNAS Direct Submission.

[1]To whom correspondence may be addressed. Email: francois.moisan@u-bordeaux.fr.

This article contains supporting information online at https://www.pnas.org/lookup/suppl/doi:10.1073/pnas.2018690118/-/DCSupplemental.

Published February 8, 2021.

different tumor types in vivo. Retrospective clinical studies have shown that β-blocker use for hypertension is associated with improved cancer-specific survival compared with patients using other types of antihypertensive medications. For instance, a beneficial effect on survival was seen in breast cancer patients receiving the nonselective β-blocker propranolol but not with the β-1 antagonist atenolol (16). Additional studies showed a benefit of β-blocker use in patients with colorectal (17, 18) and pancreatic cancer (19). A prospective nonrandomized study of propranolol in the adjuvant setting for resected melanoma found an 80% reduction in melanoma recurrence (20). However, prospective clinical evidence supporting a role for propranolol in cancer treatment or prevention is limited. It is unlikely that beta blockade becomes an anticancer drug as a monotherapy, but combination therapy seems more promising (21). In this work, our hypothesis was that the antitumor effect of propranolol in malignant tumors was related to some common feature with the IH microenvironment. Since the increase of hypoxia-induced mediators has been shown in children with hemangioma (22, 23), we speculated that a hypoxic microenvironment could trigger the propranolol antitumor effect. We therefore chose a model of human malignant tumor cells xenografted in immunocompromised mice with continuous treatment of anti–vascular endothelial growth factor-(VEGF-A) bevacizumab (Avastin), hereafter abbreviated as Bev, in order to obtain a hypoxic tumor model (24). Tumor hypoxia induced by sunitinib and bevacizumab has already been used in mouse models in order to study specific drug sensitivity induced by up-regulation of HIF-1-α hypoxia (25). Sunitinib has also been used to assess propranolol antitumor efficacy in a melanoma model (26); nonetheless, bevacizumab is a more specific antiangiogenic drug than sunitinib.

Using human malignant cell lines xenografted into immunodeficient mice as a model, we show in this study that propranolol induced the down-regulation of aquaporin-1 (AQP1), a transmembrane protein forming a channel for water and small solutes (27–30), and has a very pronounced effect on tumor growth in our mouse model (31–34). Looking for AQP1 expression in IH, we describe a special peripheral vascular layer made of dendritic cells named telocytes (TCs) with highly specific expression of AQP1, suggesting a key role in the exquisite sensitivity of IH to propranolol, which was verified in vitro with patients' cells.

Results

Propranolol Efficiently Reduces the Growth of U87 Tumors in Bev-Treated Mice. To explore propranolol antitumor efficacy in a Bev-treated mouse model, four human malignant cell lines, A375 (melanoma), A431 (skin carcinoma), CAPAN-2 (prostate cancer), and U87-MG (glioblastoma), were subcutaneously engrafted into immunocompromised NOD-SCID gamma (NSG) mice. The effect of propranolol in the Bev-treated mouse model was evaluated on tumor growth.

Antitumor activity of propranolol was evaluated in Bev-treated mice by the T/C ratio, which was calculated according to the following equation: T/C ratio = tumor weight of propranolol treated mice/mean tumor weight of placebo-treated control mice. While propranolol showed no significant antitumor activity in xenografts of A375 (melanoma), A431 (skin carcinoma), or CAPAN-2 (prostate cancer), a significant growth inhibitory effect of propranolol was measured in U87-MG (glioblastoma) xenografts. (Fig. 1*A*).

We then tested antitumor efficacy of three different doses of propranolol (i.e., 2, 10, and 50 mg/kg per day) on U87-MG xenografts in Bev-treated and non–Bev-treated mice (Fig. 1*B*). Results showed that propranolol treatment as monotherapy (without Bev) had no significant effect on U87 tumor growth (Fig. 1*B*). On the contrary, Bev alone (without propranolol) had a very pronounced antitumor effect during the first month. However, a reacceleration of tumor growth occurred afterward (Fig. 1*B*), perhaps due to the development of resistance to Bev. Interestingly, the addition of propranolol enhanced the antitumor effect of Bev and significantly inhibited reacceleration of tumor growth for the three different doses of propranolol (Fig. 1 *B* and *C*). For example, tumors treated with Bev and 2 mg/kg/day of propranolol were 42% smaller than those treated with Bev/placebo ($P < 0.0001$) (Fig. 1*B*). Of note, the high dose of propranolol (50 mg/kg/day) was less efficient than low doses (2 and 10 mg/kg/day) in inhibiting tumor growth, with only 30% smaller tumors (Fig. 1 *B* and *C* and *SI Appendix*, Fig. S1*A*), which did not correlate with VEGF expression (*SI Appendix*, Fig. S1*B*). This might be because propranolol has been found to have an inverse agonist activity in addition to its ADRB antagonist activity in a concentration-dependent manner (35–37). For the rest of the experiments, we used 2 mg/kg/day of propranolol to minimize this observed paradoxical effect.

Antitumor Effect of Propranolol Is Associated with AQP1 Down-Regulation in U87 Model. We used the U87 Bev-treated model to investigate the propranolol antitumor mechanism. To this end, we performed a differential proteomics analysis to characterize the proteins differentially expressed between xenografts treated with Bev + propranolol versus Bev + placebo versus untreated. Differential proteomics analysis revealed nine overexpressed and eight down-regulated proteins in Bev-treated xenografts compared with untreated tumors as seen in the volcano plot (Fig. 2*A* and *SI Appendix*, Table S1) (38). When U87 tumors treated with Bev + propranolol versus Bev + placebo were compared, differential protein expression profiling revealed 6 up-regulated and 10 down-regulated proteins (Fig. 2*B* and *SI Appendix*, Table S1) (38). The two volcano plots show the common modulated proteins AQP1 and α-1 type 1 collagen (COL1A1), with AQP1 being the most significantly altered when propranolol is added. Of note, AQPs are a family of transmembrane proteins with 13 members (39). They are different in their tissue distribution, although the majority are located in the epithelium and specialized cells such as erythrocytes, astrocytes, adipocytes, and ECs (39). AQPs have various known physiological roles, such as urine concentration in kidney, cell migration required for angiogenesis and wound healing, regulation of brain water homeostasis, neural signal transduction, skin moisturization, and cell proliferation in wound healing (40). We therefore focused on the role of AQP1 in tumor response to propranolol for the following reasons: First, while AQP1 protein level was up-regulated in Bev-treated U87 xenografts, its level was decreased to baseline in the Bev + propranolol group. Second, there was a significant positive correlation between tumor weight and AQP1 protein abundance in the Bev-treated group ($R^2 = 0.4279$ and $P = 0.0402$) (i.e., the higher the level of AQP1 protein, the larger the tumors on the day of euthanasia) (Fig. 2*C*). These results suggest that AQP1, whose overexpression has been recently associated with many types of cancers as a distinctive clinical prognostic factor (29, 30, 41–46), could be a promising downstream target for the beta blockade antitumor effect. To establish potential relationships between ADRB2 and AQP1, STRING functional protein association analysis (47) was performed on proteomics data. It showed that ADRB2 could be linked to AQP1 through calmodulin-2, SRC, caveolin-1, and β-catenin (Fig. 2*D*). Interestingly, carbonic Anhydrase IX (CA9), MMP10, and collagen 1, three of the nine up-regulated proteins in the Bev-treated group (Fig. 2*A* and *SI Appendix*, Table S1), were found downstream of this ADRB2/AQP1 signaling network (Fig. 2*D*).

AQP1 Is Regulated by Beta Adrenergic Pathway. We first examined the expression of both ADRB2 and AQP1 in U87 xenografts compared to propranolol-unresponsive tumors A375, A431, and CAPAN-2 (*SI Appendix*, Fig. S1*C*). Of note, among the three

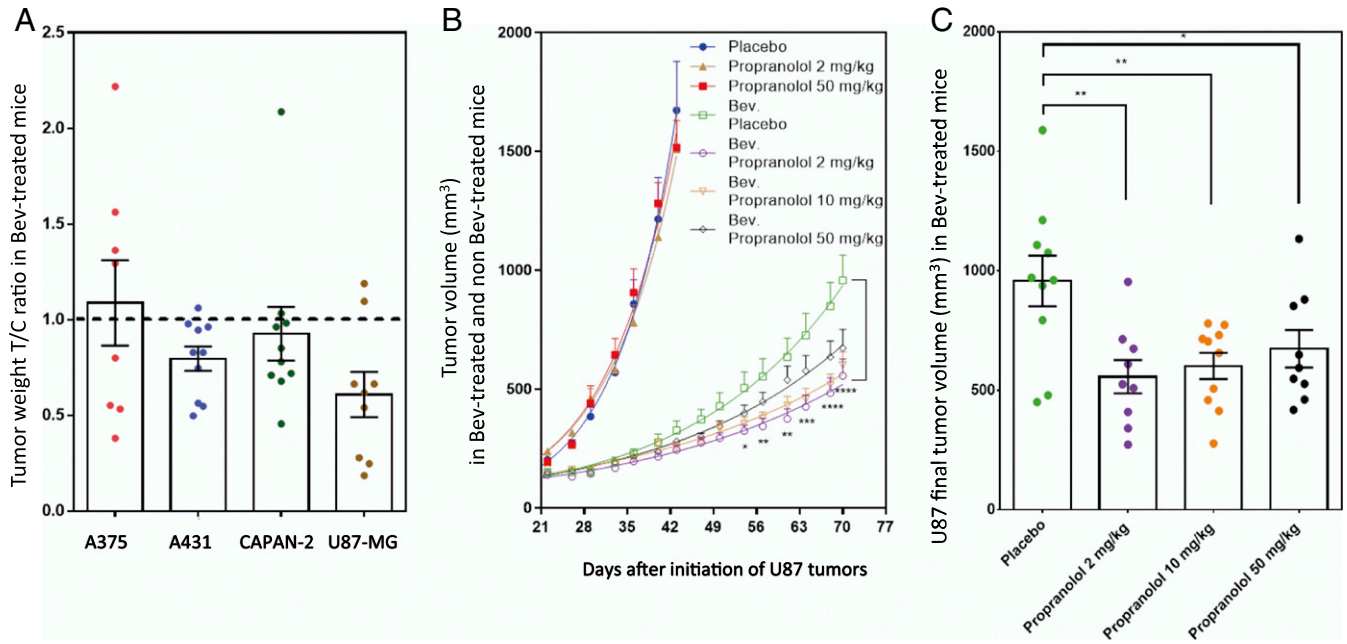

Fig. 1. Propranolol antitumor efficacy in a bevacizumab-treated mouse model. (*A*) A375 (melanoma), A431 (skin carcinoma), CAPAN-2 (prostate cancer), and U87-MG (glioblastoma) cell lines were subcutaneously transplanted into NSG mice. Antitumor growth activity of propranolol (2 mg/kg/day) was evaluated by the T/C ratio in mice under continuous treatment with 10 mg/kg twice a week of Bev. The T/C ratio was calculated according to the following equation: T/C ratio = tumor weight of propranolol treated mice/mean tumor weight of placebo-treated control mice. (*B*) U87-MG propranolol dose response (2, 10, or 50 mg/kg/day) in Bev-treated mice compared with non–Bev-treated mice. Tumor volumes were measured (mean ± SEM) at indicated times. Statistical analysis (two-way ANOVA with uncorrected Fisher's Least Significant Difference (LSD) test) compared tumor volumes in mice treated with 2 mg/kg/day of propranolol to placebo-treated mice in a Bev-treated mouse model. (*C*) The distribution of tumor volumes at day 75 after U87-MG cell transplantation into mice. Statistical analysis (two-tailed unpaired *t* test) is expressed as mean ± SEM. $n = 10$ mice per group; $^{*}P < 0.05$, $^{**}P < 0.005$, $^{***}P < 0.0005$, and $^{****}P < 0.00005$.

ADRBs, U87 cells have undetectable expression of ADRB1 and ADRB3 by qPCR (*SI Appendix*, Fig. S1*D*). We then verified whether down-regulation of ADRB2 could affect the tumorigenic properties of U87. To this end, endogenous ADRB2 protein expression in U87 cells was inhibited using lentivirus-mediated expression of short hairpin RNA (shRNA) against ADRB2. Five different shRNA targeting ADRB2 were tested; all experiments were performed with the most efficient one (later called shADRB2), which inhibited the mRNA expression of ADRB2 by 75% (*SI Appendix*, Fig. S2*A*). Both shCT- and shADRB2-transduced U87 were subcutaneously transplanted into NSG mice. In mice subjected to intraperitoneal injections of Bev (10 mg/kg, twice a week), periodic measurements of tumor volume indicated that knockdown of ADRB2 resulted in significantly decreased tumor growth. Indeed, in Bev-treated mice, the mean volume of tumors derived from shADRB2-transduced cells on day 75 after transplantation was 1,221 mm^3 ± 199 compared to 2,304 mm^3 ± 375 for tumors derived from shCT-transduced U87 ($P = 0.031$) (Fig. 3*A*). The study of tumor-specific growth rate (SGR) in non-Bev and Bev-treated mice (following the equation SGR = Ln2/doubling time) confirms that shADRB2 inhibits tumor growth in Bev-treated mice only (*SI Appendix*, Fig. S2*B*).

Differential proteomics analysis among groups revealed that the AQP1 protein level was significantly lower in tumors formed by shADRB2-transduced cells compared with those formed by shCT-transduced cells in Bev-treated mice ($P = 0.0258$) but not in phosphate-buffered saline (PBS)-treated control mice (Fig. 3*B*).

ADRB2/AQP1 Axis in Propranolol Antitumor Effect. To determine whether the observed antitumor effect of propranolol relies on the ADRB2/AQP1 axis, we tested the effect of AQP1 down-regulation in the U87 bev-treated model. Both shCT- and shAQP1-transduced U87 were transplanted into NSG mice. As in the previous experiments, treatments with placebo or propranolol were started the day after cell transplantation in Bev-treated mice. Western blotting revealed that lentivirus-mediated expression of shAQP1 stably inhibited by 77% the AQP1 expression in tumors formed by shAQP1-transduced U87 (*SI Appendix*, Fig. S2*E*). In accordance with the previous experiments, propranolol enhanced the antitumor growth effect of Bev, reflected by a twofold decrease in the weight of tumor T/C ratio compared with placebo-treated tumors (Fig. 3*C*). Likewise, AQP1 down-regulation sensitized U87 tumors to Bev treatment. Indeed, the mean weight of tumor T/C ratio composed of shAQP1-transduced cells was twofold lower compared with tumors composed of shCT-transduced cells in Bev-treated mice (Fig. 3*C* and *SI Appendix*, Fig. S2*E*). Of note, while the addition of propranolol or down-regulation of AQP1 improved the antitumor growth effect of Bev ($P = 0.0336$ and $P = 0.0149$, respectively), the combination of propranolol and shAQP1 had no additive effect on tumor growth in Bev-treated mice, with a mean tumor weight similar to that obtained by the addition of propranolol or of shAQP1 (Fig. 3*C*). This suggests that AQP1 down-regulation and propranolol treatment modulate tumor growth through the same pathway.

To further examine this hypothesis, the effect of AQP-1 up-regulation was then tested. The results showed that the volume of tumors in Bev-treated mice was higher when AQP1 expression was up-regulated (pAQP1) (Fig. 3*D* and *SI Appendix*, Fig. S2*C*). However, this increase in tumor volume was not observed when shADRB2-tranduced U87 was used (Fig. 3*D* and *SI Appendix*, Fig. S2*D*), confirming that AQP1/ADRB2 axis and propranolol treatment modulate tumor growth through the same pathway. Moreover, in both pAQP1 and control tumors (pCT), there was no additive effect of ADRB2 down-regulation (shADRB2) and

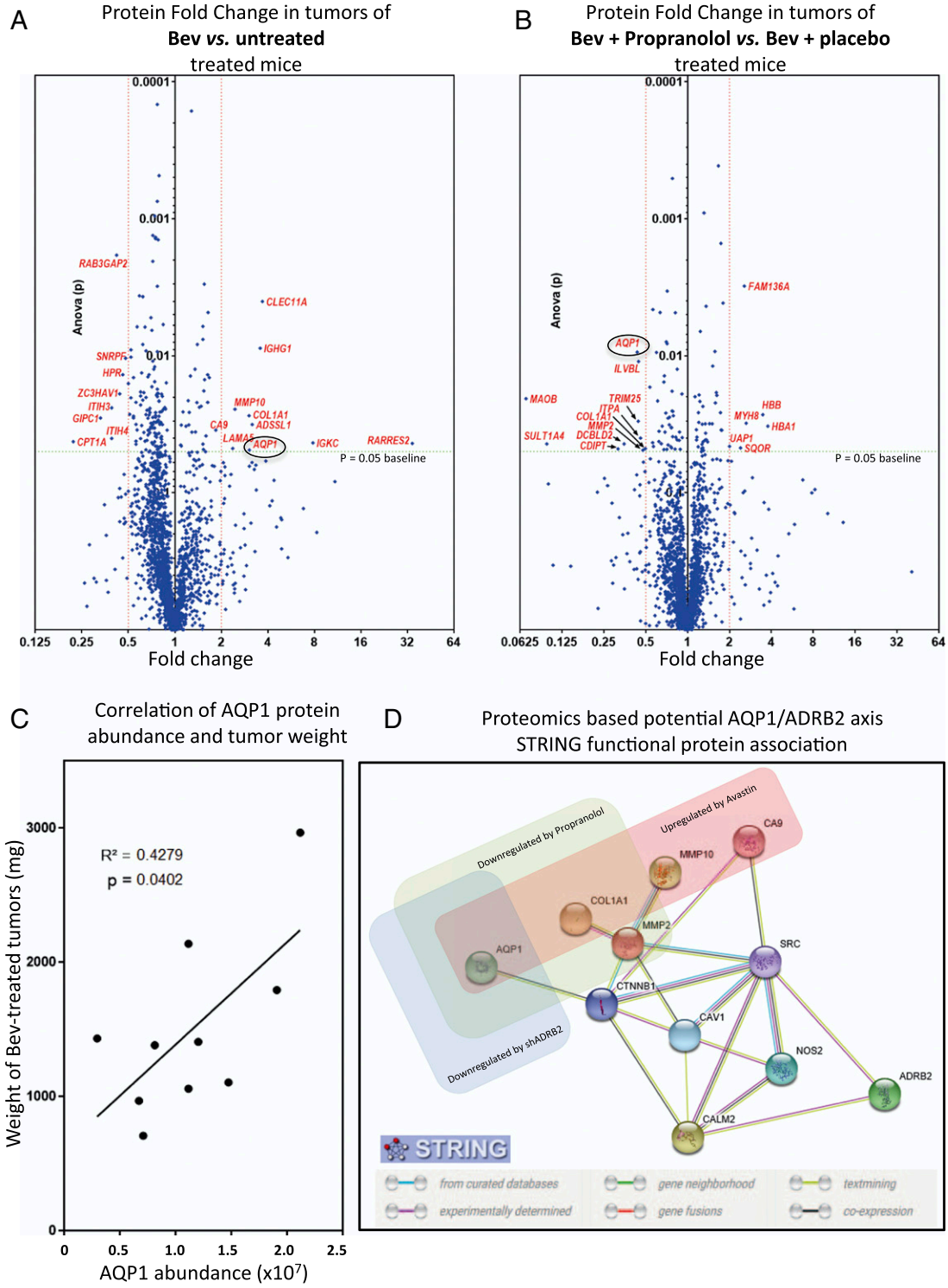

Fig. 2. AQP1 is up-regulated in Bev-treated tumors but down-regulated when propranolol is added. (*A* and *B*) U87-MG tumor xenografts treated with placebo only, Bev + placebo, or combined Bev and propranolol were subjected to proteomic analysis. Volcano plots show a comparison of fold change protein levels between placebo- and Bev-treated xenografts (*A*) and Bev + placebo– and combined (Bev + propranolol)-treated xenografts (*B*). Proteins with a mean protein abundance altered by a factor of two or more and $P > 0.05$ (ANOVA) have their name in red. The protein with the most statically different mean abundance when propranolol was added was AQP1. (*C*) Pearson correlation analysis showing a significant positive correlation between AQP1 protein abundance and tumor weight (milligrams) in Bev-treated mice. The calculation of protein abundance (sum of the volume of corresponding human peptides) is shown. (*D*) Potential ADRB2-AQP1 interaction network. STRING functional protein association, based on proteome data of nontreated, Bev-treated, Bev plus propranolol-treated U87 tumors, as well as proteomic data from Bev-treated xenografts, formed by shCT- and shADRB2-transduced U87. Proteins significantly up-regulated in Bev-treated U87 tumors are boxed in red. Proteins significantly down-regulated in xenografts treated with Bev plus propranolol are boxed in green. Proteins significantly down-regulated in Bev-treated xenografts formed by transplantation of shADRB2-transduced U87 are boxed in blue. MMP10 = matrix metalloproteinase 10; MMP2 = type IV collagenase (angiogenesis); CTNNB1 = β-catenin; CAV1 = Caveolin-1; CALM2 = Calmodulin-2; NOS2 = nitric oxide synthase, inducible. The STRING consortium database 2017 of known and predicted protein-protein interactions was used for interaction network prediction.

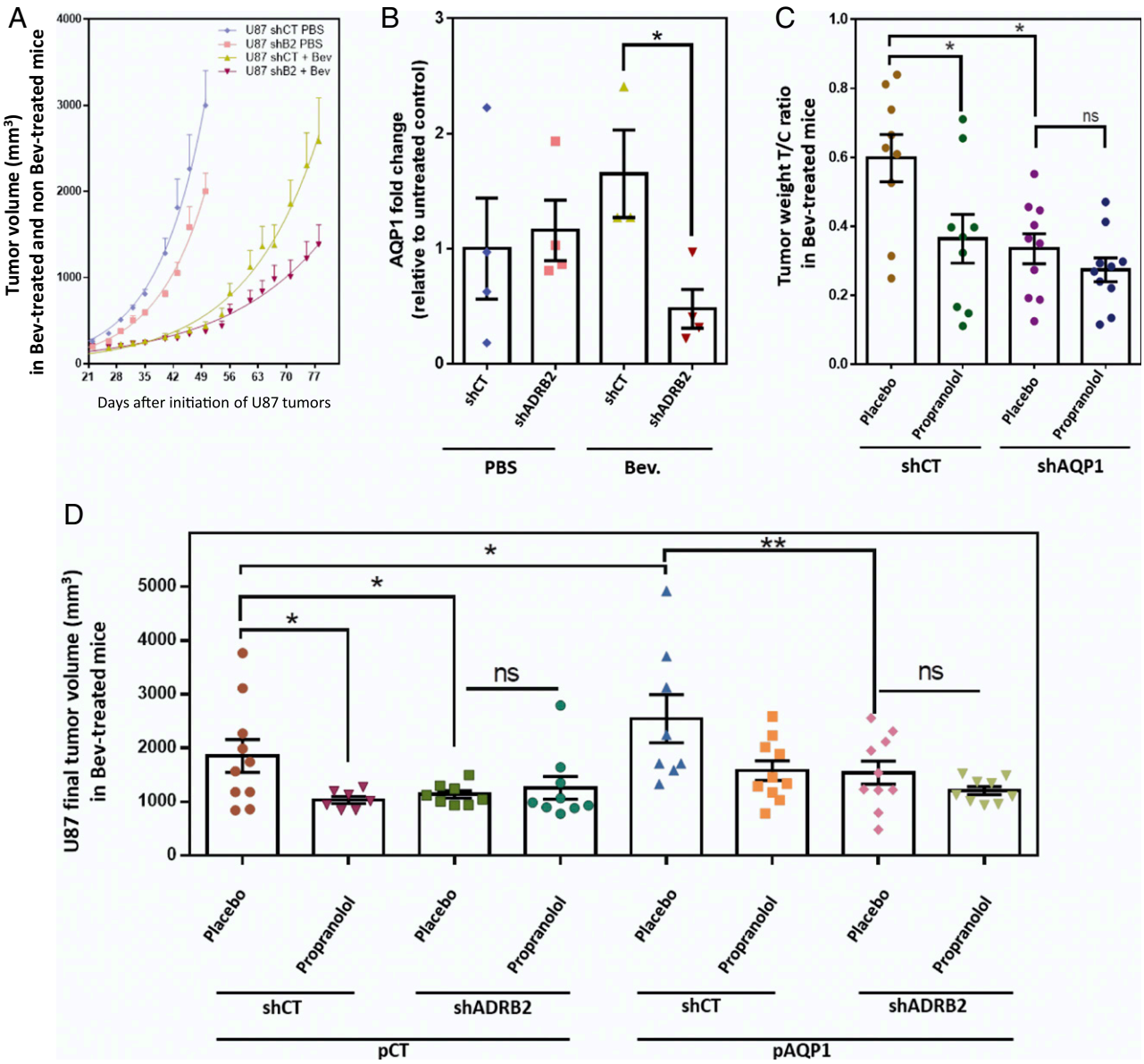

Fig. 3. ADRB2-AQP1 axis in propranolol antitumor response using U87 cells transduced with shCT, shADRB2, shAQP1, pCT, and pAQP1 were transplanted into NSG mice. (*A*) Xenograft tumors of shCT or shADRB2 U87-transduced cells were subjected to periodic measurements of tumor volume in Bev- and non–Bev-treated mice. (*B*) Collected tumors from shCT or shADRB2 U87-transduced cells were subjected to proteomic analysis. The AQP1 level was compared among the groups. Data are presented as mean with SEM relative to untreated control abundance. The calculation of protein abundance (sum of the volume of corresponding human peptides) is shown. (*C*) Xenograft tumors of U87-transduced cells with shCT or shAQP1. Antitumor growth activities of propranolol and shAQP1 were evaluated by the T/C ratio, which was calculated according to the following equation: T/C ratio= tumor weight of Bev-treated mouse/mean tumor weight of counterpart non–Bev-treated control mice (same shRNA). (*D*) Xenograft tumors of U87 cells transduced with shCT or shADRB2 and pCT or pAQP1 overexpression vector. Final tumor volumes were compared at day 85, expressed as mean ± SEM. Statistical analysis was performed with one-way ANOVA with uncorrected Fisher's LSD. $n = 10$ mice per group; $*P < 0.05$, $**P < 0.005$; ns, not significant.

propranolol treatment, confirming that propranolol effect is at least partially due to an on-target beta blockade effect.

AQP1 Has a Unique Histologic Profile in IHs Revealing a Specific Implication of Human TCs. Following the identification of AQP1 as a downstream target of propranolol in our U87 mouse model, we wondered whether AQP1 could be a marker of propranolol response in IH. To this end, the AQP1 expression profile was assessed using immunofluorescence staining on a panel of IHs; congenital hemangiomas such as noninvolutive congenital hemangiomas (NICH), partially involutive congenital hemangiomas (PICH), and rapidly involutive congenital hemangiomas (RICH) (which are typically nonresponsive to propranolol treatment); and infant normal foreskin dermis (Fig. 4 and *SI Appendix*, Figs. S3, S4, and Table S2). The results showed that IH has a unique AQP1 profile compared to nonpropranolol-responsive congenital hemangiomas or normal skin. Although IH is a capillary tumor, during the natural evolution of the tumor, vascular structures acquire bigger lumen and three layers. Indeed, while $CD31^+$/$CD34^+$ EC (tunica intima) and alpha smooth muscle actin (α-SMA^+) smooth muscle cells or pericytes (PER) (tunica media) in IHs were negative for AQP1, $CD31^-$/$CD34^+$ perivascular cells of the innermost layer of tunica adventitia stained positively for AQP1 (Fig. 4 *A*–*C* and *E* and *SI Appendix*, Figs. S3 and S5). On the contrary, ECs and perivascular cells were respectively positive and negative for AQP1 in infant normal dermis (Fig. 4*D*)

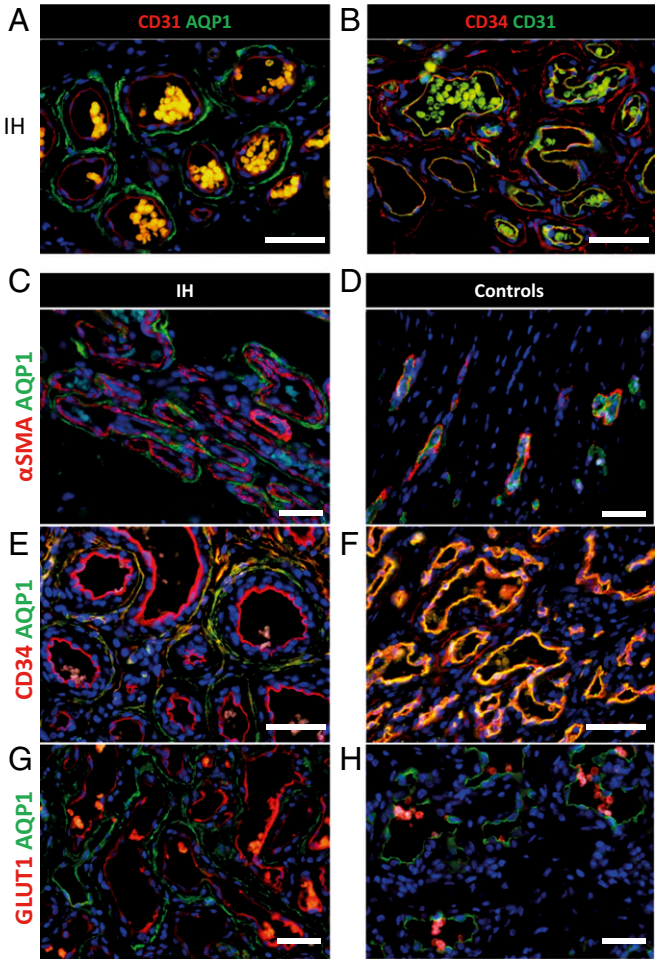

Fig. 4. AQP1 unique expression profile differentiates IHs from congenital hemangiomas. (*A*) ECs in IH are positive for CD31 marker (red staining) but negative for AQP1 (green staining). Perivascular stromal cells are positive for AQP1 but negative for CD31. (*B*) ECs in IH are positive for CD31 marker (green staining) and co-stain with CD34 (red staining). Perivascular stromal cells are positive for CD34 but negative for CD31. (*C*) PERs in IH are positive for α-SMA (red staining) but negative for AQP1 (green staining). Perivascular stromal cells are negative for α-SMA but positive for AQP1. (*D*) PERs in normal dermis are positive for α-SMA (red staining) but negative for AQP1 (green staining). ECs are negative for α-SMA and positive for AQP1. (*E*) ECs in IH are positive for CD34 marker (red staining) but negative for AQP1 (green staining). Perivascular stromal cells are positive for CD34 and co-stain with AQP1. (*F*) ECs in RICH congenital hemangioma are positive for CD34 marker (red staining) and co-stain with AQP1 (green staining). Perivascular stromal cells are positive for CD34 but negative or low for AQP1. (*G*) ECs in IH are positive for GLUT1 marker (red staining) but negative for AQP1 (green staining). Perivascular stromal cells are positive for AQP1 but negative for GLUT1. (*H*) ECs in RICH congenital hemangioma are negative for GLUT1 marker (red staining) but positive for AQP1 (green staining). Perivascular stromal cells are negative for GLUT1 and negative or low for AQP1 (red blood cells coexpress GLUT1 and AQP1).

or congenital hemangiomas (NICH, PICH, and RICH) (Fig. 4 *F* and *H* and *SI Appendix*, Figs. S3, S4, and S7). Thus, the AQP1 profile expression is a differential marker between IHs and NICH/PICH/RICH in addition to GLUT1 EC positivity; indeed, IH lesional GLUT1$^+$ ECs are found to be AQP1$^-$, and GLUT1$^-$ ECs are found to be AQP1$^+$ (48) (Fig. 4 *G* and *H* and *SI Appendix*, Figs. S7, S8, and Table S2). To further determine whether these cells could be a potential target of propranolol in IHs, their expression of ADRB2 was analyzed. Immunostaining showed that AQP1-positive perivascular cells were also positive for ADRB2 (*SI Appendix*, Fig. S8*C*).

Finally, we further characterized these perivascular cells. The specific shape of these cells with very long prolongations, a perivascular location, and CD34-positive staining suggest that they belong to a particular cell type, TCs. Morphologically, TCs have a small cell body and specific long prolongations (telopodes), with thin segments (podomers) alternating dilations (podoms) (49). TCs have been described in the interstitium of many organs. In the dermis, TCs are located around the blood vessels, sweat glands, and nerves (50) and have been defined in skin as CD34$^+$/PDGFR-α$^+$/vimentin$^+$ and CD31$^-$/CD68$^-$/CD163$^-$/c-KIT$^-$/α-SMA$^-$ cells (51). Importantly, vesicle-shedding properties have been noted in the vicinity of other interstitial cells such as mast cells (52) that are abundant and of an interesting nature in IH pathophysiology (53, 54). So far, only electron microscopy can confirm a TC cell type. Therefore, their characterization in IH was performed using transmission electron microscopy. Their very long (tens to hundreds of micrometers) and very thin podomers and telopodes as well as their stromal synapses with mast cells (Fig. 5 *A*–*C* and *SI Appendix*, Fig. S9) confirmed that AQP1-positive perivascular cells in IH are TCs. We tested AQP1-positive perivascular cells in IH for markers expressed by dermal TCs. In addition to CD34, TCs in IHs were positive for PDGFR-α and vimentin (Fig. 5*C*). They were partially positive for VEGF-A and K_i-67, indicating that TCs in IHs are proliferative and proangiogenic (Fig. 5*C*). Finally, they were negative for c-KIT, Tryptase, CD133, CD68, and CD163 (Fig. 5*C*).

IH Sensitivity to Propranolol Relies on a Cross Talk between Vascular Cells and Perivascular TCs. Given the potential importance of TCs in pathophysiology of IH, we wondered whether propranolol could affect the level of AQP1 in IH-TC. To answer this question, IH-TC were isolated from IH patients. We first checked the expression of the different markers. The results showed that the isolated cell populations were homogeneously positive for PDGFR-α, AQP1, and CD34 but negative for CD31 (Fig. 5*D*). Of note, in culture, IH-TC maintained very long and very thin prolongations typical morphology (Fig. 5*E*) as well as higher AQP1 protein levels than CH-TC or foreskin control-TC (Fig. 5*F*).

To examine the functional importance of TC in the pathophysiology of IH, we next developed a Matrigel-based angiogenesis assay, in which three cell types of interest were incorporated (i.e., IH-EC, IH-PER, and IH-TC). To this end, all three cell types were isolated from the IH fresh tissues using magnetic beads coupled with antibodies against CD31, CD34, and CD146 (as explained in *Materials and Methods* and *SI Appendix*, Fig. S10). These sorted cells were then labeled with three different fluorescent dyes: EC in red, TC in green, PER in blue. The cells were then homogeneously seeded on microslide wells covered with a thin layer of Matrigel. Tube formation was imaged 4 h later, and several angiogenesis parameters (including total tubes, total tube length, and the tube-covered area) were then analyzed. The results showed that propranolol significantly decreased the total number of tubes (27% less tubes when 3 μM propranolol was added) (Fig. 6 *A* and *B*). Similar results were obtained when 10 μM propranolol was added (Fig. 6 *A* and *B*) (n = 3; confirmed with cells from three different patients, including multiple angiogenesis parameters).

Then, we investigated the relationship between propranolol response and IH-TC–specific properties; we first replaced them with primary foreskin-TC. The results showed that the anti-angiogenic effect of propranolol was lost using foreskin-TC (Fig. 6 *A* and *B*). Finally, to see whether propranolol can affect angiogenesis parameters when IH-TC is used alone, a single cell–type angiogenesis assay was used. Of interest, no major effect of propranolol on tubulogenesis were found when IH-EC, IH-PER, and IH-TC cells were used separately (*SI Appendix*, Fig. S11*A*). Altogether, these results suggest that the sensitivity of IH to propranolol relies on a cross talk between IH-EC, IH-

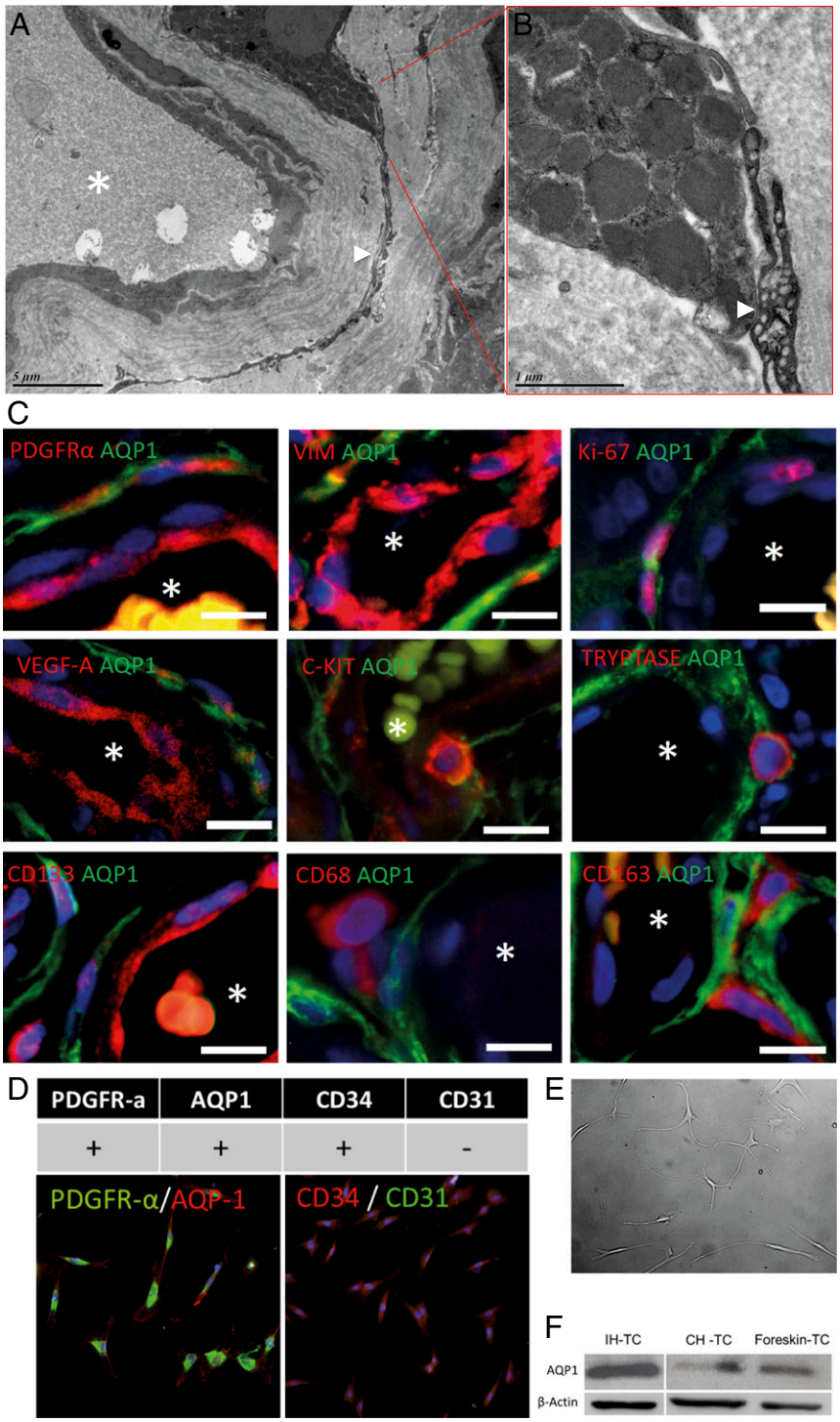

Fig. 5. AQP1-positive in IH are TCs. (*A*) Transmission electron microscopy shows a TC with a very long and thin telopode in IHs, which is connected to a mast cell by stromal synapses (*B*), confirming that these CD34+/AQP1+ cells are TCs. (*C*) TC immunophenotyping was assessed using immunofluorescence staining of PDGFR-α, vimentin, K_i-67, VEGF-A, c-KIT, Tryptase, CD133, CD68, and CD163. Nuclei were marked in blue with DAPI. Vessel lumen is marked with a white asterisk. (*D*) In vitro phenotyping of TCs was done by immune-cyto-fluorescence; TCs are homogeneously PDGFR-α, AQP1, and CD34 positive and CD31 negative. (*E*) Cultured IH-TC photograph. (*F*) AQP1 protein level in IH-TC, CH-TC (congenital hemangioma-TC), or foreskin control-TC, evaluated by Western blot (β-actin is used as loading control).

PER, and IH-TC. We then sought to determine whether the AQP1 protein level in TC was sensitive to propranolol, as observed in our in vivo model. The AQP1 protein level was evaluated in IH-TCs that had been treated for 2 h with 3 μM propranolol in the same culture conditions as the tubulogenesis assays. The results showed a significant reduction of the AQP1 level in propranolol-treated IH-TC (quantification is the mean of $n = 3$ experiments) (Fig. 6*C*). Finally, tubulogenesis assay was used to examine the functional link between AQP1 and propranolol treatment. To this end, AQP1 was down-regulated in

https://doi.org/10.1073/pnas.2018690118

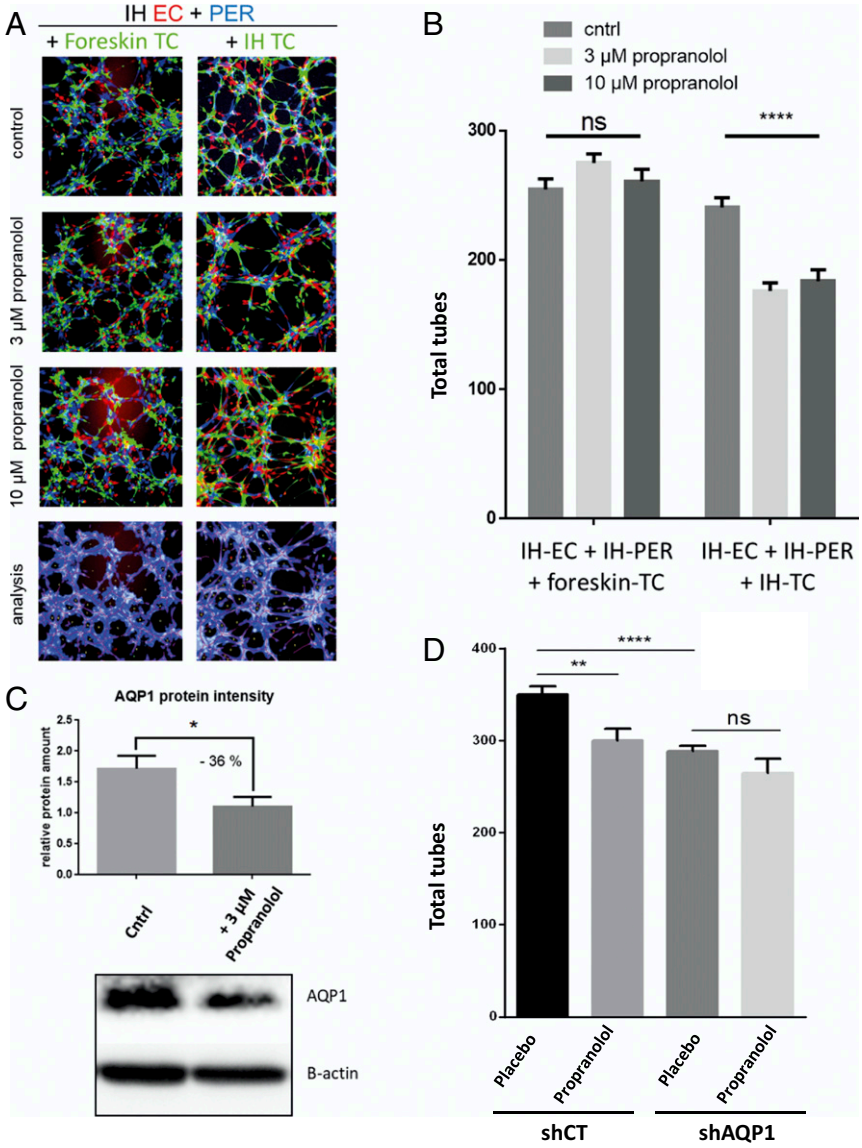

Fig. 6. The effect of propranolol on the tubulogenic properties of the combined IH-derived EC, PER, and TC depends on IH-TC. Isolated IH cells are cultured and amplified before they were labeled with three different fluorescent dyes: EC in red, PER in blue, and TC in green. EC, PER, and TC were seeded on microslide wells covered with a thin layer of Matrigel. Tube formation was then imaged 4 h later and analyzed using Wimtube software from Wimasis. (*A* and *B*) Substitution of IH-TC by foreskin-TC impaired the responses of the three-cell-type model of IH to 3 and 10 μM of propranolol. (*A*) Representative fluorescent images with illustrative analysis image. (*B*) Total tubes, average quantification of three wells per condition ($n = 3$), representative results from three different patients ($n = 3$). (*C*) Western blotting evaluation of AQP1 protein level in IH-TC in control medium or after 2 h with 3 μM propranolol. Protein intensity was normalized to β-actin. The mean relative protein amount was calculated based on three different experiments ($n = 3$). (*D*) AQP1 in IH-TC was down-regulated using shAQP1. Then, shCT- and shAQP1-transduced TCs were used in our in vitro three-cell-type–based tubulogenesis assay. Data are expressed as mean ± SEM. Statistical analysis was performed with one-way ANOVA with uncorrected Fisher's LSD. *$P < 0.05$, **$P < 0.005$, and ****$P < 0.00005$; ns, not significant.

IH-TC through the transduction of a lentiviral vector encoding shRNA targeting AQP1 (efficiency was checked by Western blot, *SI Appendix*, Fig. S11*B*). These cells were then subjected to our three-cell-type–based tubulogenesis assay. The results showed that AQP1 knockdown significantly decreased the total number of tubes and that adding propranolol on these cells did not led to a more pronounced effect (Fig. 6*D*), confirming that AQP1 and propranolol treatment modulate tube formation through the same pathway.

Discussion

This study provides insight into the antitumor pathway of propranolol and strongly suggests a link between AQP1 expression and propranolol sensitivity in malignant and benign tumors. Indeed, in our mouse experiments, only the U87 Bev-treated model with increased AQP1 was sensitive to propranolol; moreover, our results on hemangiomas show that IHs, which are sensitive to propranolol, present a $GLUT1^{+}/AQP1^{-}$ endothelium and $GLUT1^{-}/AQP1^{+}$ perivascular TCs. On the contrary, congenial hemangiomas (NICH, PICH, and RICH), which do not respond to propranolol, have a $GLUT1^{-}/AQP1^{+}$ endothelium and $GLUT1^{-}/AQP1^{-}$ perivascular TCs. The $GLUT1^{+}/AQP1^{-}$ endothelium with a specific perivascular positive for AQP1 (and AQP4) located in astrocytes (44) is a known feature of the blood–brain barrier (BBB) in the central nervous system (CNS) and brain tumors such as glioblastomas (44, 55). BBB

astrocytes are known to be responsible for the negative regulation of AQP1 in ECs (56).

It has been shown that the expression of AQP1 is up-regulated in many cancers (30) and some brain tumors, notably glioblastomas (44, 57, 58). AQP1 expression in glioblastomas has been found to be induced by growth factors, D-glucose, and hypoxia (44, 59). Consistently, we found that AQP1 is up-regulated in Bev-treated U87 xenografts (Fig. 2*A*), where relative hypoxia is induced by antiangiogenic effect of the anti–VEGF-A antibody bevacizumab (34). As evidence of the induction of hypoxia in Bev-treated xenografts, elevated levels of CA9, a marker of hypoxia, as well as of some proangiogenic factors associated with hypoxia such as VEGF were detected by qPCR (*SI Appendix*, Fig. S1*B*) and MMP2/10 in our proteomics analysis (Fig. 2 and *SI Appendix*, Table S1). Some of those hypoxia-related markers elevated in our Bev-treated model have been associated with the pathophysiology of IH (22, 23, 60), which might explain why their presence is associated with propranolol tumor response in our model. It is also interesting to note that COL1A1 was coregulated with AQP1; a functional link may exist between AQP1, COL1A1, and metalloproteinases, as they are all part of extracellular matrix remodeling. Indeed, physiological and pathological functional links have been shown in the literature (28, 30, 61). Then, our results showed that AQP1 down-regulation by propranolol treatment or shAQP1 significantly decreased the exponential growth phase of Bev-treated U87 tumors (Figs. 1*B*, 2*B*, and 3*C*). We observed a significant antitumor effect of propranolol at doses of 2 and 10 mg/kg/day under this regimen. However, the 50 mg/kg/day dose of propranolol was less efficient, which is interesting in regard to dose response on VEGF expression (Fig. 1 *B* and *C* and *SI Appendix*, Fig. S1*A*). This paradoxical effect has also been described with propranolol in an osteoporosis animal model (62, 63) and may be attributed to the interaction of high doses of propranolol with different types of adrenergic receptors and/or the concentration-dependent inverse agonist activity of propranolol on ADRB. This observation is important because the majority of studies to date on the mechanism of action of propranolol used very high doses, ranging from 50 to 200 μM in vitro (64–68). Moreover, it has been shown that 100 nM is sufficient to reach a maximum plateau in binding ADRB2 (69). Given that the plasma concentration of propranolol in IH patients after oral administration of one of the two daily doses of propranolol (3 mg/kg) varies between 21.3 and 125 ng/mL (0.48 μM) (10), it is very unlikely that the effect of propranolol in IH can be mimicked and studied with 100× doses.

Little is known about the relationship between ADRBs and AQPs. Nonetheless, treatment of frog skin with isoproterenol, a nonselective ADRB agonist, was reported to be associated with water permeability, whereas propranolol had an inhibitory effect (70). Both events are mediated by AQPs, which are translocated to the apical membrane (70). Moreover, agonists of β2 adrenoreceptor, terbutaline and salbutamol, respectively, in human monocytic cell line or in vivo in rat up-regulated AQP1 (71, 72). In our xenograft model, propranolol treatment was as efficient as AQP1 silencing in reducing Bev-treated tumor growth, and no additive effect was observed (Fig. 3*C*). Moreover, when propranolol treatment combined with ADRB2 silencing was tested, no additive effect was found (Fig. 3*D*), suggesting that the antitumor effect of propranolol is the result of an on-target ADRB2 effect. Our functional protein association networks analysis as well as AQP1 silencing and overexpression further suggest that AQP1 regulation and propranolol treatment have a common pathway in our xenograft model (Fig. 2*D*). Indeed, although AQP1 has been described as a distinctive clinical prognostic factor in cancers (30) and we further confirmed the protumor effect of its overexpression in vivo (Fig. 3*D*), its silencing alone had no antitumor effect in non–Bev-treated mice in our model but greatly sensitized U87 tumors to Bev with a magnitude comparable to that of propranolol treatment or ADRB2 down-regulation (Fig. 3 *C* and *D*). Of note, the antiangiogenic effect of AQP1 silencing has been shown to be increased by hypoxia and/or VEGF-neutralizing antibody; in other words, AQP1 is required for hypoxia-inducible angiogenesis (73).

Given the importance of AQP1 for propranolol response in our xenograft tumor model, we looked for the cell expressing AQP1 in IH. Interstitial perivascular TCs, which are numerous in IH, are highly positive for AQP1 compared to congenital hemangiomas or normal dermis (Figs. 4 and 5*F*). The effects of TCs on skin homeostasis, including neonatal blood–skin barrier, skin remodeling, skin regeneration, and skin repair could be a part of the pathomechanism of IH leading to its rapid growth and its natural or propranolol-induced involution (50, 74, 75). Moreover, IH-TCs make contacts known as stromal synapses with the numerous mast cells present in IH, as evidenced by many vesicles observed at the level of the stromal synapses (Fig. 5 *A*–*C* and *SI Appendix*, Fig. S8), allowing a paracrine cell–cell dialogue (50, 76). Interestingly, we were able to reproduce the propranolol effect on the AQP1 levels seen in the U87 mouse model on cultured IH-TCs as well (Fig. 6*C*). Moreover, our in vitro angiogenesis assays showed that propranolol significantly decreased angiogenesis parameters when IH-TC were mixed with IH-EC and IH-PER (Fig. 6). Of note, this effect was lost if IH-TC was replaced with foreskin-TC or if each cell type was used separately (Fig. 6 and *SI Appendix*, Fig. S11). Furthermore, down-regulation of AQP1 in IH-TCs significantly decreased angiogenesis parameters and abrogated the effect of propranolol on in vitro tube formation (Fig. 6*D*). Altogether, these results suggest that the exquisite sensitivity of IH to propranolol relies on a cross talk between the three cell types with a critical role of AQP1-positive IH-TC. The role of AQP1 as a marker of propranolol response should be further investigated to identify tumor types with potential therapeutic benefits of beta blockade.

Materials and Methods

Drugs and Chemicals. Clinical formulations of bevacizumab Avastin (Roche) and propranolol (Karnodyl, Primius Lab Ltd) were purchased from the Bordeaux Hospital Pharmacy. The infantile propranolol formulation Hemangeol and placebo were provided by Laboratoire Pierre Fabre Medicament, France.

Human Samples. All studies were performed in accordance with the Declaration of Helsinki. Human samples were obtained from patients seen at Bordeaux University Hospital. All donors provided written informed consent. The Ethics Committee of Bordeaux University Hospital (CE-GP-2019-23) approved the study.

Animals and Experimental Protocol. NSG mice were bred in standard conditions compliant with regulations and housed in a pathogen-free animal facility. All mouse experiments were carried out with the approval of Bordeaux University Animal Care and Use Committee. Male mice were used in all experiments. Mice were randomly assigned to each group before the start, and experiments were performed blinded with respect to treatment. Experimental subgroups consisted of 10 mice per group, with each subgroup caged separately. A total of 5×10^5 of U87-MG tumor cells combined with Matrigel matrix high concentration (Corning) were subcutaneously injected in the right flank of mice. For the Bev-treated mouse model (Bev is a humanized anti-VEGF monoclonal antibody), Bev (intraperitoneal injections of 10 mg/kg, twice a week) and propranolol (Hemangeol, Pierre Fabre Pharmaceuticals, Inc., Parsippany, NJ) (ranging from 2, 10, or 50 mg/kg/day in drinking water, renewed three times a week) treatments were started the day after transplantation of human tumor cells. Counterpart control groups received Bev and the Hemangeol vehicle solution in drinking water (placebo). To assess the tumor volumes and growth rate of tumors, caliper measurements of the tumors were obtained twice a week. Tumor volumes were calculated by the following formula: volume = (width) 2 × length/2. After 2.5 mo of treatment, mice were euthanized and tumors were extracted, weighted, and collected for immunohistochemical studies and RNA and protein purification.

Cell Lines and Culture. A375 (melanoma), A431 (skin carcinoma), CAPAN-2 (prostate cancer), and U87-MG (glioblastoma) were obtained from the American Type Culture Collection (ATCC; http://www.atcc.org/). The U87-MG line was derived from malignant gliomas of a male patient. The cell line is likely a glioblastoma of CNS origin (77). Cells were grown in Dulbecco's Modified Eagle's Medium (DMEM) supplemented with 10% fetal calf serum (Gibco; Thermo Fisher Scientific, Waltham, MA) and cultured in a humidified atmosphere of 5% CO_2 at 37 °C. U87-MG cell cultures were tested every 2 wk for mycoplasma contamination by PCR.

Cytogenetic Verification. To examine the cytogenetic profile of U-87 MG, cells were cultured in Labtek chamber slides (Thermo Fisher Scientific). After 2 d, mitotic divisions were blocked at the (pro)metaphasic stage by adding a colcemid solution for 3 h (KaryoMAX Colcemid solution at 0.10 μg/mL; Life Technologies Corporation). Hypotonic shock and fixation of the chromosome preparations were performed with a saline solution (1% sodium citrate) and Carnoy's solution (acetic acid and methanol, 1:3 volume/volume), respectively.

Conventional karyotyping of U-87 MG cells was performed after Giemsa staining and heat denaturation ("R-bands"). Conventional karyotyping of U-87 MG cells identified structural abnormalities previously described in this cell line, including additional material of unknown origin on chromosomes 1 and 6, partial deletions of chromosomes 9 and 18, and a derivative chromosome from a translocation involving the long arm of chromosome 10 and the short arm of chromosome 16 (chromosome der(10;16)(q10;q10)); data are from the Physical Sciences-Oncology Network Bioresource Core Facility (PBCF) at ATCC.

Driver mutation information is as follows: CDKN2A homozygous c.1_471del471, phosphatase and Tensin homolog (PTEN) homozygous c.209+1G > T, CDKN2C homozygous c.1_507del507, p53 wild type. The mutation data were obtained from the Sanger Institute Catalogue of Somatic Mutations in Cancer website (https://cancer.sanger.ac.uk/cell_lines/sample/overview?id=687590).

Immunohistochemistry and Fluorescence. Following deparaffinization of formalin-fixed, paraffin-embedded tissue sections, antigen was retrieved by using citrate buffer pH6 in a PT Link instrument (Dako, Agilent). The sections were then incubated overnight at 4 °C with primary antibodies (*SI Appendix*, Table S3). After incubation for 1 h with conjugated secondary antibody, the nuclei were counterstained with DAPI.

IH Cell Sorting. After mechanical disruption and enzyme digestion of IH fresh tissues with a mixture of collagenase (Sigma-Aldrich) and dispase (Sigma-Aldrich) in sterile PBS, single cell suspensions were purified with a sequential sorting using a column-based magnetic cell separation technology according to the manufacturer's recommendations (*SI Appendix*, Fig. S9). ECs, TCs, and PERs were isolated by sequential sorting, first with anti-CD31 (EC), then anti-CD34 (TC), and finally anti-CD146 (PER) coupled to magnetic beads (Miltenyi). ECs were cultured in endothelial growth medium (EGM2, Promocell), TC in DMEM (Gibco) supplemented with 10% fetal bovine serum, and PER in Pericyte growth medium (Promocell), all supplemented with 1% penicillin-streptomycin.

In Vitro Matrigel Tube Formation Assay. Matrigel Growth Factor Reduced Basement Membrane Matrix (Corning) was polymerized for 30 min at room temperature and then 1 h at 37 °C on μ-slide angiogenesis wells (Ibidi). Sorted IH-EC, HI-PER and IH-TC were, respectively, labeled with CMRA-548 orange dye, CellTrace-405 violet dye and CMFDA-492 green dye (Thermo Fisher). IH-derived cells were suspended in 50 μL endothelial growth medium (EGM2, Promocell) containing 10 μM noradrenaline (Mylan) and 3 or 10 μM propranolol (Karnodyl, Primius Lab Ltd). Cells from each type were seeded separately or together onto Matrigel in triplicate (10,000 cells/well or 3,200 EC + 3,200 TC + 3,200 PER/well). μ-slides were incubated for 4 h at 37° C. After incubation, tube formation was imaged at 10× magnification using an Eclipse microscope (Nikon). The angiogenesis parameters, including total tubes, total tube length, percentage of covered area, total loops, and nets, were analyzed using the image analysis software Wimasis WimTube (Onimagin Technologies). The mean value of three images taken per well was obtained for each condition in triplicate.

Statistical Analyses. Equal variance was checked for each comparison using an F-test. The standard two-tailed Student's *t* test for two data sets or ANOVA (Fisher's test) with more than two data sets was used, except in Fig. 3*D* for comparisons between the following groups: "placebo shCT pCT" versus "propranolol shCT pCT" or versus "placebo shADRB2 pCT;" because of significantly different variance, Welch's unequal variances *t* test was used instead. Analyses were performed using Prism V6 and V8 (GraphPad Inc.). Data are presented as means ± SEM.

Data Availability. The data supporting the findings of this study are available within the article text and its supporting information. The mass spectrometry proteomics data have been deposited to the ProteomeXchange Consortium via the Proteomics Identifications Database partner repository with the dataset identifier PXD021457 (http://www.ebi.ac.uk/pride/archive/projects/PXD021457) (38).

ACKNOWLEDGMENTS. A.T. gratefully acknowledges support from the Agence nationale de la recherche (ANR), Ligue Nationale contre le Cancer, L'Oreal La Roche Posay, Laboratoires Pierre Fabre with a special mention to Dr. Jean-Jacques Voisard for his continous support, "Fondation de l'Avenir," and "Fondation Association pour la Recherche contre le Cancer." Electron microscopy studies were conducted at the Bordeaux Imaging Center–Bordeaux University, a core facility of the national infrastructure "France BioImaging" (ANR-10-INBS-04 FranceBioImaging). We thank VectUb of Bordeaux University for preparing lentiviral particles. We are grateful to R. Cooke for copyediting the manuscript and L. R. Salmy from Bordeaux University, Institut de Santé Publique, d'Epidémiologie et de Développement (ISPED), Centre INSERM U897-Epidemiologie-Biostatistique, for statistical analysis support. Source funding was received through ANR "BETASKIN2" ANR-12-BSV1-0021-01.

1. C. Léauté-Labrèze *et al.*, A randomized, controlled trial of oral propranolol in infantile hemangioma. *N. Engl. J. Med.* **372**, 735–746 (2015).
2. D. M. Rosenbaum, S. G. F. Rasmussen, B. K. Kobilka, The structure and function of G-protein-coupled receptors. *Nature* **459**, 356–363 (2009).
3. H. M. Schuller, B. Cole, Regulation of cell proliferation by beta-adrenergic receptors in a human lung adenocarcinoma cell line. *Carcinogenesis* **10**, 1753–1755 (1989).
4. C. Léauté-Labrèze *et al.*, Propranolol for severe hemangiomas of infancy. *N. Engl. J. Med.* **358**, 2649–2651 (2008).
5. S. Greenberger, J. Bischoff, Infantile hemangioma-mechanism(s) of drug action on a vascular tumor. *Cold Spring Harb. Perspect. Med.* **1**, a006460 (2011).
6. C. H. Storch, P. H. Hoeger, Propranolol for infantile haemangiomas: Insights into the molecular mechanisms of action. *Br. J. Dermatol.* **163**, 269–274 (2010).
7. J. Stiles *et al.*, Propranolol treatment of infantile hemangioma endothelial cells: A molecular analysis. *Exp. Ther. Med.* **4**, 594–604 (2012).
8. H. Chim *et al.*, Propranolol induces regression of hemangioma cells through HIF-1α-mediated inhibition of VEGF-A. *Ann. Surg.* **256**, 146–156 (2012).
9. A. Wong *et al.*, Propranolol accelerates adipogenesis in hemangioma stem cells and causes apoptosis of hemangioma endothelial cells. *Plast. Reconstr. Surg.* **130**, 1012–1021 (2012).
10. L. Del Frari *et al.*, Propranolol pharmacokinetics in infants treated for Infantile Hemangiomas requiring systemic therapy: Modeling and dosing regimen recommendations. *Pharmacol. Res. Perspect.* **6**, e00399 (2018).
11. D. Xu *et al.*, Isolation, characterization, and in vitro propagation of infantile hemangioma stem cells and an in vivo mouse model. *J. Hematol. Oncol.* **4**, 54 (2011).
12. D. M. Smadja, J. B. Mulliken, J. Bischoff, E-selectin mediates stem cell adhesion and formation of blood vessels in a murine model of infantile hemangioma. *Am. J. Pathol.* **181**, 2239–2247 (2012).
13. Z. A. Z. A. Khan *et al.*, Multipotential stem cells recapitulate human infantile hemangioma in immunodeficient mice. *J. Clin. Invest.* **118**, 2592–2599 (2008).
14. H. M. Mai *et al.*, CD133 selected stem cells from proliferating infantile hemangioma and establishment of an in vivo mice model of hemangioma. *Chin. Med. J. (Engl.)* **126**, 88–94 (2013).
15. D. Lee *et al.*, Propranolol targets the contractility of infantile haemangioma-derived pericytes. *Br. J. Dermatol.* **171**, 1129–1137 (2014).
16. P. Pantziarka, B. A. Bryan, S. Crispino, E. B. Dickerson, Propranolol and breast cancer-a work in progress. *Ecancermedicalscience* **12**, ed82 (2018).
17. P. Tsui *et al.*, Generation, characterization and biological activity of CCL2 (MCP-1/JE) and CCL12 (MCP-5) specific antibodies. *Hum. Antibodies* **16**, 117–125 (2007).
18. L. Jansen, M. Hoffmeister, V. Arndt, J. Chang-Claude, H. Brenner, Stage-specific associations between beta blocker use and prognosis after colorectal cancer. *Cancer* **120**, 1178–1186 (2014).
19. M. S. Beg *et al.*, Impact of concurrent medication use on pancreatic cancer survival-SEER-medicare analysis. *Am. J. Clin. Oncol.* **41**, 766–771 (2018).
20. V. De Giorgi *et al.*, Propranolol for off-label treatment of patients with melanoma: Results from a cohort study. *JAMA Oncol.* **4**, e172908 (2018).
21. P. Pantziarka *et al.*, Repurposing drugs in oncology (ReDO)-Propranolol as an anti-cancer agent. *Ecancermedicalscience* **10**, 680 (2016).
22. M. E. Kleinman *et al.*, Hypoxia-induced mediators of stem/progenitor cell trafficking are increased in children with hemangioma. *Arterioscler. Thromb. Vasc. Biol.* **27**, 2664–2670 (2007).
23. G. Chen *et al.*, Hypoxia-induced autophagy in endothelial cells: A double-edged sword in the progression of infantile haemangioma? *Cardiovasc. Res.* **98**, 437–448 (2013).

24. K. Kumar *et al*., Dichloroacetate reverses the hypoxic adaptation to bevacizumab and enhances its antitumor effects in mouse xenografts. *J. Mol. Med. (Berl.)* **91**, 749–758 (2013).
25. J. Hartwich *et al*., HIF-1α activation mediates resistance to anti-angiogenic therapy in neuroblastoma xenografts. *J. Pediatr. Surg.* **48**, 39–46 (2013).
26. X. Kuang *et al*., Propranolol enhanced the anti-tumor effect of sunitinib by inhibiting proliferation and inducing G0/G1/S phase arrest in malignant melanoma. *Oncotarget* **9**, 802–811 (2017).
27. E. Monzani, R. Bazzotti, C. Perego, C. A. M. La Porta, AQP1 is not only a water channel: It contributes to cell migration through Lin7/beta-catenin. *PLoS One* **4**, e6167 (2009).
28. J. Wang *et al*., Aquaporins as diagnostic and therapeutic targets in cancer: How far we are? *J. Transl. Med.* **13**, 96 (2015).
29. J. Hu, A. S. Verkman, Increased migration and metastatic potential of tumor cells expressing aquaporin water channels. *FASEB J.* **20**, 1892–1894 (2006).
30. Y. Tomita *et al*., Role of aquaporin 1 signalling in cancer development and progression. *Int. J. Mol. Sci.* **18**, 299 (2017).
31. S. Miyazaki *et al*., Anti-VEGF antibody therapy induces tumor hypoxia and stanniocalcin 2 expression and potentiates growth of human colon cancer xenografts. *Int. J. Cancer* **135**, 295–307 (2014).
32. A. Rapisarda *et al*., Increased antitumor activity of bevacizumab in combination with hypoxia inducible factor-1 inhibition. *Mol. Cancer Ther.* **8**, 1867–1877 (2009).
33. A. McIntyre *et al*., Carbonic anhydrase IX promotes tumor growth and necrosis in vivo and inhibition enhances anti-VEGF therapy. *Clin. Cancer Res.* **18**, 3100–3111 (2012).
34. R. Kuang *et al*., GLUT3 upregulation promotes metabolic reprogramming associated with antiangiogenic therapy resistance. *JCI Insight* **2**, e88815 (2017).
35. J. G. Baker, I. P. Hall, S. J. Hill, Agonist and inverse agonist actions of beta-blockers at the human beta 2-adrenoceptor provide evidence for agonist-directed signaling. *Mol. Pharmacol.* **64**, 1357–1369 (2003).
36. P. Chidiac, T. E. Hebert, M. Valiquette, M. Dennis, M. Bouvier, Inverse agonist activity of beta-adrenergic antagonists. *Mol. Pharmacol.* **45**, 490–499 (1994).
37. G. Khilnani, A. K. Khilnani, Inverse agonism and its therapeutic significance. *Indian J. Pharmacol.* **43**, 492–501 (2011).
38. F. Moisan *et al*., Critical role of Aquaporin-1 and telocytes in infantile hemangioma response to propranolol. ProteomeXchange Consortium. http://www.ebi.ac.uk/pride/archive/projects/PXD021457. Deposited 25 January 2021.
39. R. E. Day *et al*., Human aquaporins: Regulators of transcellular water flow. *Biochim. Biophys. Acta* **1840**, 1492–1506 (2014).
40. M. Boury-Jamot *et al*., "Skin aquaporins: Function in hydration, wound healing, and skin epidermis homeostasis" in *Aquaporins. Handbook of Experimental Pharmacology*, E. Beitz, Ed. (Springer, Berlin, Heidelberg, 2009), 190, https://doi.org/10.1007/978-3-540-79885-9_10.
41. Z. Wu *et al*., RNAi-mediated silencing of AQP1 expression inhibited the proliferation, invasion and tumorigenesis of osteosarcoma cells. *Cancer Biol. Ther.* **16**, 1332–1340 (2015).
42. R. C. Huebert *et al*., Aquaporin-1 promotes angiogenesis, fibrosis, and portal hypertension through mechanisms dependent on osmotically sensitive microRNAs. *Am. J. Pathol.* **179**, 1851–1860 (2011).
43. C. Esteva-Font, B.-J. Jin, A. S. Verkman, Aquaporin-1 gene deletion reduces breast tumor growth and lung metastasis in tumor-producing MMTV-PyVT mice. *FASEB J.* **28**, 1446–1453 (2014).
44. Y. Hayashi, N. A. Edwards, M. A. Proescholdt, E. H. Oldfield, M. J. Merrill, Regulation and function of aquaporin-1 in glioma cells. *Neoplasia* **9**, 777–787 (2007).
45. F. D. Martinez, P. E. Graves, M. Baldini, S. Solomon, R. Erickson, Association between genetic polymorphisms of the beta2-adrenoceptor and response to albuterol in children with and without a history of wheezing. *J. Clin. Invest.* **100**, 3184–3188 (1997).
46. P. Deb *et al*., Correlation of expression pattern of aquaporin-1 in primary central nervous system tumors with tumor type, grade, proliferation, microvessel density, contrast-enhancement and perilesional edema. *J. Cancer Res. Ther.* **8**, 571–577 (2012).
47. D. Szklarczyk *et al*., STRING v10: Protein-protein interaction networks, integrated over the tree of life. *Nucleic Acids Res.* **43**, D447–D452 (2015).
48. P. E. North, M. Waner, A. Mizeracki, M. C. Mihm, Jr, GLUT1: A newly discovered immunohistochemical marker for juvenile hemangiomas. *Hum. Pathol.* **31**, 11–22 (2000).
49. L. M. Popescu, M.-S. Faussone-Pellegrini, TELOCYTES–A case of serendipity: The winding way from interstitial cells of cajal (ICC), via interstitial cajal-like cells (ICLC) to TELOCYTES. *J. Cell. Mol. Med.* **14**, 729–740 (2010).
50. L. Ceafalan, M. Gherghiceanu, L. M. Popescu, O. Simionescu, Telocytes in human skin–Are they involved in skin regeneration? *J. Cell. Mol. Med.* **16**, 1405–1420 (2012).
51. M. Manetti *et al*., Evidence for progressive reduction and loss of telocytes in the dermal cellular network of systemic sclerosis. *J. Cell. Mol. Med.* **17**, 482–496 (2013).
52. M. C. Rusu *et al*., Skin telocytes. *Ann. Anat.* **194**, 359–367 (2012).
53. T. Itinteang *et al*., Mast cells in infantile haemangioma possess a primitive myeloid phenotype. *J. Clin. Pathol.* **66**, 597–600 (2013).
54. S. Prey *et al*., Mast cells as possible targets of propranolol therapy: An immunohistological study of beta-adrenergic receptors in infantile haemangiomas. *Histopathology* **65**, 436–439 (2014).
55. S. Nagamatsu, H. Sawa, A. Wakizaka, T. Hoshino, Expression of facilitative glucose transporter isoforms in human brain tumors. *J. Neurochem.* **61**, 2048–2053 (1993).
56. D. Dolman, S. Drndarski, N. J. Abbott, M. Rattray, Induction of aquaporin 1 but not aquaporin 4 messenger RNA in rat primary brain microvessel endothelial cells in culture. *J. Neurochem.* **93**, 825–833 (2005).
57. J. M. Markert *et al*., Differential gene expression profiling in human brain tumors. *Physiol. Genomics* **5**, 21–33 (2001).
58. K. Oshio *et al*., Expression of the aquaporin-1 water channel in human glial tumors. *Neurosurgery* **56**, 375–381, discussion 375–381 (2005).
59. W. Meng *et al*., Hypoxia-induced up-regulation of aquaporin-1 in rat schwann cells via the MAPK pathway. *Int. J. Clin. Exp. Med.* **10**, 9271–9276 (2017).
60. C. J. Kleber *et al*., Urinary matrix metalloproteinases-2/9 in healthy infants and haemangioma patients prior to and during propranolol therapy. *Eur. J. Pediatr.* **171**, 941–946 (2012).
61. J. Steinberg *et al*., Integrative epigenomics, transcriptomics and proteomics of patient chondrocytes reveal genes and pathways involved in osteoarthritis. *Sci. Rep.* **7**, 8935 (2017).
62. N. Bonnet *et al*., Dose effects of propranolol on cancellous and cortical bone in ovariectomized adult rats. *J. Pharmacol. Exp. Ther.* **318**, 1118–1127 (2006).
63. W. F. Rodrigues *et al*., Low dose of propranolol down-modulates bone resorption by inhibiting inflammation and osteoclast differentiation. *Br. J. Pharmacol.* **165**, 2140–2151 (2012).
64. Y. Z. Chen *et al*., Propranolol inhibits the proliferation, migration and tube formation of hemangioma cells through HIF-1α dependent mechanisms. *Braz. J. Med. Biol. Res.* **50**, e6138 (2017).
65. X. Liao *et al*., The β-adrenoceptor antagonist, propranolol, induces human gastric cancer cell apoptosis and cell cycle arrest via inhibiting nuclear factor κB signaling. *Oncol. Rep.* **24**, 1669–1676 (2010).
66. F. Hajighasemi, A. Mirshafiey, In vitro sensitivity of leukemia cells to propranolol. *J. Clin. Med. Res.* **1**, 144–149 (2009).
67. W.-J. Wei, C.-T. Shen, H.-J. Song, Z.-L. Qiu, Q.-Y. Luo, Propranolol sensitizes thyroid cancer cells to cytotoxic effect of vemurafenib. *Oncol. Rep.* **36**, 1576–1584 (2016).
68. N. C. O. Munabi *et al*., Propranolol targets hemangioma stem cells via cAMP and mitogen-activated protein kinase regulation. *Stem Cells Transl. Med.* **5**, 45–55 (2016).
69. D. C. Alcobia *et al*., Visualizing Ligand binding to a GPCR in vivo using NanoBRET. *iScience* **6**, 280–288 (2018).
70. Y. Ogushi, D. Kitagawa, T. Hasegawa, M. Suzuki, S. Tanaka, Correlation between aquaporin and water permeability in response to vasotocin, hydrin and beta-adrenergic effectors in the ventral pelvic skin of the tree frog Hyla japonica. *J. Exp. Biol.* **213**, 288–294 (2010).
71. K. Rump *et al*., Aquaporin 1 and 5 expression evoked by the β2 adrenoreceptor agonist terbutaline and lipopolysaccharide in mice and in the human monocytic cell line THP-1 is differentially regulated. *Shock* **40**, 430–436 (2013).
72. C. Uhlig *et al*., The effects of salbutamol on epithelial ion channels depend on the etiology of acute respiratory distress syndrome but not the route of administration. *Respir. Res.* **15**, 56 (2014).
73. K. Kaneko *et al*., Aquaporin 1 is required for hypoxia-inducible angiogenesis in human retinal vascular endothelial cells. *Microvasc. Res.* **75**, 297–301 (2008).
74. N. Mirancea, A.-M. Moroşanu, G.-V. Mirancea, F. D. Juravle, V. S. Mănoiu, Infrastructure of the telocytes from tumor stroma in the skin basal and squamous cell carcinomas. *Rom. J. Morphol. Embryol.* **54**, 1025–1037 (2013).
75. C. G. Manole, M. Gherghiceanu, O. Simionescu, Telocyte dynamics in psoriasis. *J. Cell. Mol. Med.* **19**, 1504–1519 (2015).
76. J. Yang, Y. Li, F. Xue, W. Liu, S. Zhang, Exosomes derived from cardiac telocytes exert positive effects on endothelial cells. *Am. J. Transl. Res.* **9**, 5375–5387 (2017).
77. M. Allen, M. Bjerke, H. Edlund, S. Nelander, B. Westermark, Origin of the U87MG glioma cell line: Good news and bad news. *Sci. Transl. Med.* **8**, 354re3 (2016).